Transactions of the Korean Nuclear Society Spring Meeting
Jeju, Korea, May 19-20, 2022

Evaluation method of thermal properties of fuel deposits simulated in PWR primary water condition

Hee-Sang Shim [a*], Hye Min Park [a,b], Hyeong Wook Kim [a,c], Young-Kook Lee [b], Jeongho Han [c], Do Haeng Hur [a]
[a]*Materials Safety Technology Development Division, Korea Atomic Energy Research Institute, 989-111 Daedeok-daero, Yuseong-gu, Daejeon 34057, Korea*
[b]*Department of Advanced Materials Engineering, Yonsei University,50 Yonsei-ro, Seodaemun-gu, Seoul 03722, Korea*
[c]*Division of Materials Science & Engineering, Hanyang University,222 Wangsimni-ro, Seongdong-gu, Seoul 03722, Korea*
[*]*Corresponding author: hshim@kaeri.re.kr*

1. Introduction

Many nuclear power plants have recently been employing strategies for the power uprate, high burn-up, and long-term operation for economical electricity generation [1,2]. These operation strategies result increase in the thickness of fuel cladding oxide and the amount of fuel deposit (or crud). Actually, the oxide thickness of zirconium alloy cladding has reached to acceptable limit (less than 100 μm) during normal operation due to increased licensed limit of fuel burn-up with recent operating strategies. In addition, the crud-induced power shift (CIPS) and crud-induced localized corrosion (CILC), which threaten seriously fuel integrity, have continuously occurred with increase of fuel crud thickness [3]. Several power shift events, which are caused by boron accumulation into porous crud matrix, have occurred 12 times in domestic nuclear power plants since 1990. However, CILC, which is caused by an increase in the thermal resistance of fuel due to localized crud deposition, has occurred at 4 US nuclear power plants but has not been reported in domestic power plants [4]. This is probably because the analysis of damaged fuel cladding is much difficult that must be performed in a special environment using a hot cell.

Recently, nuclear regulatory agencies such as KINS or NRC are strengthening the fuel safety criteria for design basis accidents such as loss of coolant accident (LOCA) or reactivity initiated accident (RIA) because the thickness increase of fuel cladding oxide and crud can affect more seriously to the fuel integrity in accident conditions than normal operation condition [5]. In addition, they have demand to reflect the actual thermal resistances of fuel cladding oxide and crud, which have previously used with a constant value or a calculated value, into the computation code for evaluating fuel integrity. However, a measurement and a calculation of thermal resistance of crud layer are not simple because the crud consists of complex chemical composition and various geometry as well as deposited on curved surface. Thereby, few studies have been conducted on the measurement of crud's thermal properties [6-8].

In this study, in order to reduce the analysis error of thermal properties, crud layer of nickel ferrite was deposited on flat plate having same properties with commercial fuel cladding under simulated primary condition. The density, specific heat capacity and thermal diffusivity of curd layer were measured using pycnometer, differential scanning calorimetry (DSC), and laser flash analyzer (LFA) as a function of temperature. In addition, we calculate the thermal conductivity of crud layer as a function of temperature from measured characteristic values.

2. Experimental

Porous crud layers were deposited on Zr1.0Nb-1.0Sn-0.1Fe metallic plates using a simulated primary loop with controlling heater temperature. Heater to control the heat flux of metallic plate with a dimension of 10 mm x 10 mm x 0.48 mmt was specially designed as shown in Fig. 1. Prior to crud deposition, the specimen is cleaned with ultrasonication in acetone, alcohol and deionized water for each 10 min. The plate specimen was mounted on heater surface and it was inserted into the test section. The primary water was prepared by dissolving LiOH of 2 ppm and H_3BO_3 of 1,000 ppm into deionized water. The dissolved oxygen and hydrogen concentration in coolant were controlled to be less than 5 ppb and remained at 35 cc/kg·H_2O, respectively. The primary water was circulated with flow rate of 100 cc/min. The crud source was prepared by dissolving 600 ppm of nickel ethylenediamine tetraaccetic acid (EDTA) and 800 ppm of iron acetate into deionized water. The crud source solution was supplied to test section at an injection rate of 1.0 cc/min when the coolant temperature and pressure in test section was stabilized at 328°C and at 130 bar, respectively. The surface temperature of metallic substrate surface was maintained at 345, 350, and 355°C, respectively, in order to control the boiling condition. Then, the heat flux was calculated with 5.3, 6.1, 6.8 W/cm^2 for 345, 350 and 355°C, respectively, from Gunther's equation. The crud deposition was performed for 25 days.

To investigate the porosity effect on thermal conductivity of crud layer, dense crud film having chemical composition and thickness similar with those of porous crud were prepared using RF-magnetron sputtering system. Sputtering was performed using both NiO and Fe_3O_4 targets under argon gas at 300°C for 112 h. The RF power of NiO and Fe_3O_4 targets was controlled to 100W and 400 W, respectively. The dense crud was deposited to be a thickness of 50 μm.

The surface morphology and chemical composition of cruds deposited on fuel cladding material were observed using a scanning electron microscope (SEM) equipped with energy dispersive spectroscopy (EDS). The cross-sectional images of cruds were measured using focused ion beam (FIB)-SEM. Crystallinity of cruds were analyzed using X-ray diffraction (XRD). Thermal diffusivity, specific heat capacity and density were measured using LFA, DSC and He gas pycnometer, respectively. The thermal conductivity (λ) of cruds were obtained by multiplying the thermal diffusivity (α), specific heat capacity (c_p), and density (ρ).

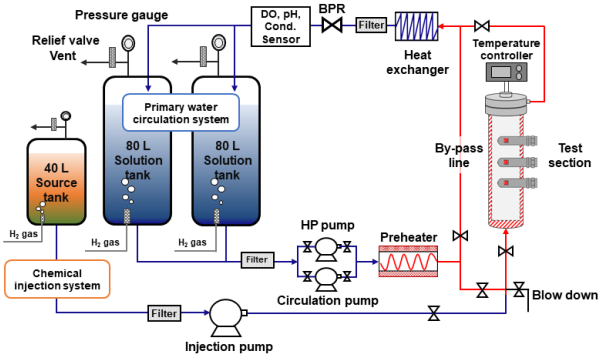

Fig. 1. A Schematic of the simulated crud deposition loop

3. Results & discussion

Fig. 2 shows the SEM surface images of dense and porous cruds. The surface of dense crud coated using co-sputtering is very clean and smooth as shown in Fig. 2(a), although it is observed in enlarged scale comparing other images. However, cruds deposited in simulated PWR primary loop show a rough surface, which consists of many protruding structures and holes as shown in Figs. 2(b)-2(d). This is probably because crud layers are deposited under boiling condition. The protrusion density of crud surface slightly increases as the surface temperature of substrate increases.

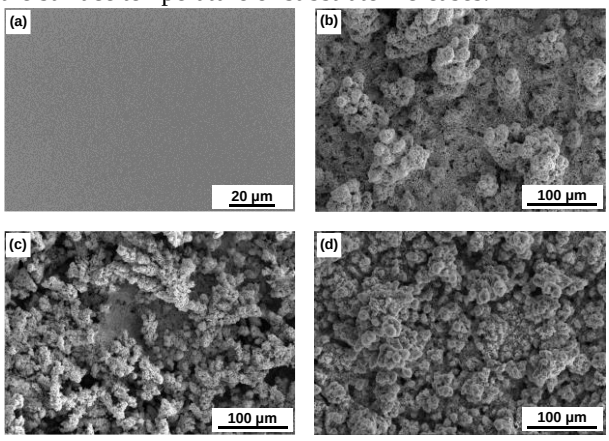

Fig. 2. SEM surface micrographs of (a) dense crud and porous cruds deposited at the specimen surface temperature of (b) 345°C, (c) 350°C and (d) 355°C.

Fig. 3 shows the enlarged SEM surface images and EDS analysis results of cruds. The sputter-deposited crud shows slightly uneven surface, while the cruds deposited in PWR primary loop are composed of polyhedral particles with sized of hundreds nanometer to few micrometers. The chemical composition of four crud samples was analyzed as a nickel ferrite to be $Ni_{0.7}Fe_{2.3}O_4$.

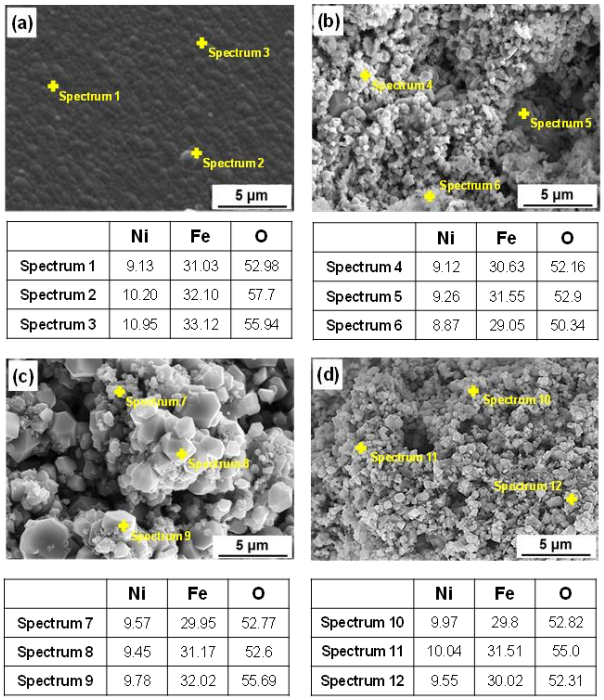

	Ni	Fe	O
Spectrum 1	9.13	31.03	52.98
Spectrum 2	10.20	32.10	57.7
Spectrum 3	10.95	33.12	55.94

	Ni	Fe	O
Spectrum 4	9.12	30.63	52.16
Spectrum 5	9.26	31.55	52.9
Spectrum 6	8.87	29.05	50.34

	Ni	Fe	O
Spectrum 7	9.57	29.95	52.77
Spectrum 8	9.45	31.17	52.6
Spectrum 9	9.78	32.02	55.69

	Ni	Fe	O
Spectrum 10	9.97	29.8	52.82
Spectrum 11	10.04	31.51	55.0
Spectrum 12	9.55	30.02	52.31

Fig. 3. Surface SEM micrographs and EDS point analysis of (a) dense crud and porous cruds deposited at the specimen surface temperature of (b) 345°C, (c) 350°C and (d) 355°C.

Fig. 4 displays the cross-sectional SEM images of cruds deposited using sputtering and crud deposition loop. To analyze average porosity and thickness of crud layers, the specimens were prepared by splitting the crud sputtered on silicon wafer and by machining cruds deposited in PWR primary loop with FIB, respectively. The pore is not observed in sputter-deposited crud layer and it is dense film with uniform thickness of ca. 50 μm as shown in Fig. 4(a). However, cruds deposited in PWR primary loop shows different thickness for the location and pores having various size as shown in Figs. 4(b)-4(d). The average porosity and thickness of four crud layers are compared together in Fig.5. Average porosity is measured by 0% for dense film and by 22.5% for 345°C crud, 27.3% for 350°C crud and 31.0% for 355°C crud, respectively. This means that the porosity of crud increases with increasing heater temperature due to the activation of boiling, which is one of the root causes for crud deposition.

Fig. 6 shows the X-ray diffraction patterns of crud layers. Herein, crud samples were renamed with porosity value such as P0, P22, P27 and P31. Four crud layers are a non-stoichiometric nickel ferrite ($Ni_xFe_{3-x}O_4$) and the characteristic peas of XRD patterns for those cruds were consistent with the standard pattern of cubic spinel $Ni_{0.4}Fe_{2.6}O_4$ (JCPDS Card No. 87-2338).

Although the stoichiometry in XRD data is slightly different from that in SEM-EDS, it is sure that all four crud specimens had the same crystallinity.

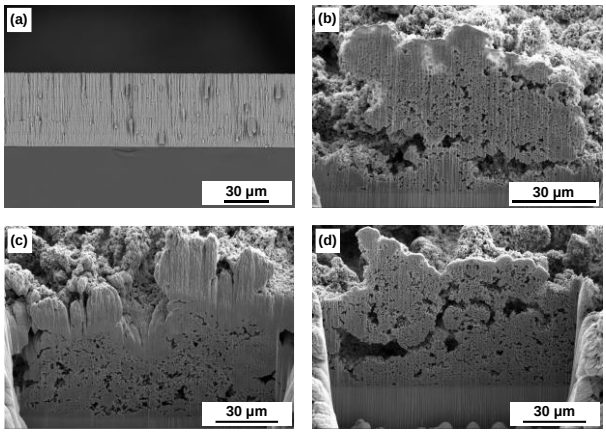

Fig. 4. SEM cross-sectional micrographs of (a) dense crud and porous cruds deposited at the specimen surface temperature of (b) 345℃, (c) 350℃ and (d) 355℃.

Fig. 7 shows the density and specific heat capacity of the dense crud as a function of temperature. The density measured using He gas pycnometer decreases with increasing the temperature as shown in Fig. 7(a). However, the specific heat capacity of nickel ferrite crud shows a transition of λ shape at 833 K, which is similar with Ziemniak's result for $NiFe_2O_4$ powder [9]. It is well known that the λ transition is caused by magnetic property change of nickel ferrite. It is understood that the difference of 26.5 K in transition temperature is caused by stoichiometric difference. The density and specific heat capacity of cruds deposited in PWR primary loop could not be measured due to those porous structures. Thus, the same values with that of dense crud were used to calculate the thermal conductivity.

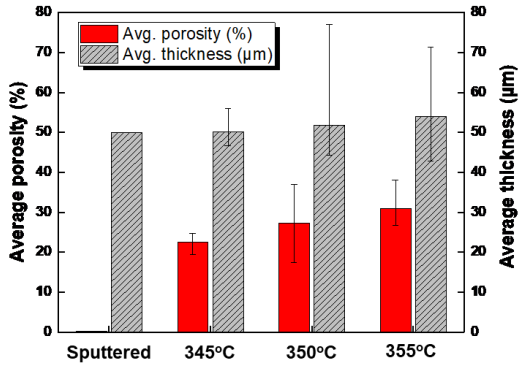

Fig. 5. Average porosity and thickness of crud layers measured from FIB-SEM images.

Fig. 8 displays the thermal diffusivity and thermal conductivity of zirconium alloy cruds with different porosity as a function of temperature. Thermal diffusivity of zirconium alloy metal exponentially increases but that of crud decreases with increasing the temperature as shown in Fig. 8(a). Thermal diffusivity of zirconium alloy metal is larger by 7 times with 7.394 mm^2/s at 473 K than that of dense crud with 1.143 mm^2/s. The diffusivity of crud decreases about 70% with increase in porosity from 1.143 mm^2/s to 0.37 mm^2/s at 473 K. This means that the thermal resistance of crud layer increases due to increased porosity.

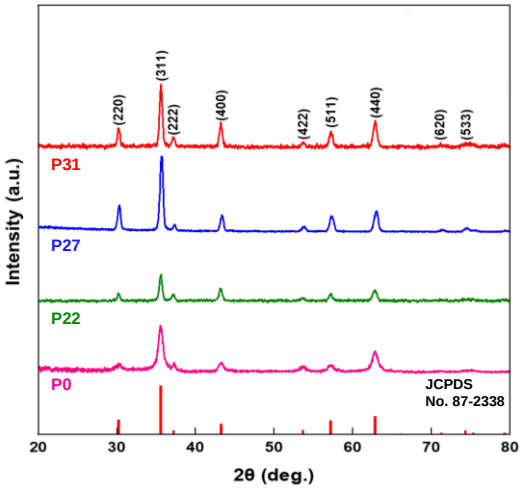

Fig. 6. XRD patterns of dense and porous cruds deposited on zirconium alloy plate.

Fig. 8(b) shows the thermal conductivity of zirconium alloy metal and cruds with different porosity, which is calculated by multiple of density, specific heat capacity and thermal diffusivity. Thermal conductivity of zirconium alloy metal also increases exponentially as a function of temperature. While thermal conductivity of cruds decreases with increasing the temperature similar with the tendency of thermal diffusivity. Thermal conductivity of zirconium alloy is larger by 2.7 times with 11.96 W/m·K at 473K than that of dense crud with 4.39 W/m·K. Thermal conductivity of crud with 31% porosity decreases by 70% with 1.53 W/m·K at 473 K from that of dense crud.

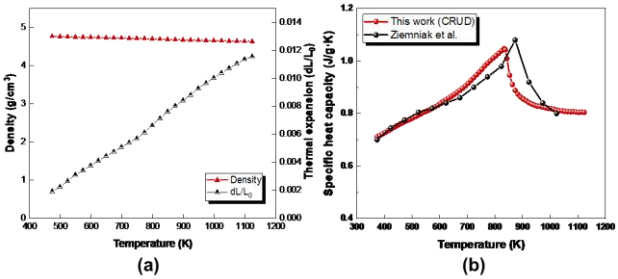

Fig. 7. (a) Density and (b) specific heat capacity of sputter-deposited crud in the temperature range from 473K to 1123K.

However, thermal conductivity of crud having 27% porosity offsets from the tendency of other crud specimens. It remains constant value up to 870 K and slightly increases at the temperature higher than 870 K. This can be seen that the porous structure of crud

having 27% porosity is destroyed during analysis from the SEM surface images before and after analysis as not shown here.

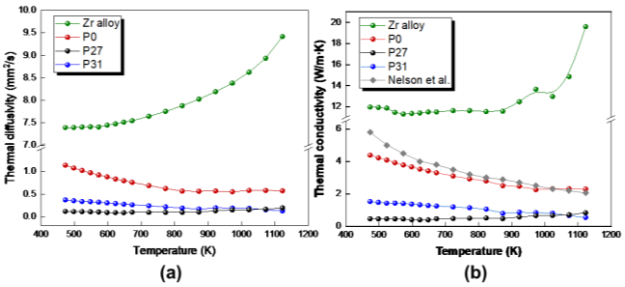

Fig. 8. (a) Thermal diffusivity and (b) thermal conductivity of zirconium ally and cruds with different porosity in the temperature range from 473K to 1123K.

In Fig. 8(b), thermal conductivity of nickel ferrite ($NiFe_2O_4$) having 5% porosity, which is reported by Nelson et al., is compared with our data [10]. This is similar value with that of dense crud but shows more abrupt decrease with increasing the temperature. It is probably to be caused by its porosity.

4. Conclusions

We have investigated thermal properties of cruds having different porosity fabricated using sputtering system and simulated PWR primary loop in this work. All crud layer is a non-stoichiometric spinel nickel ferrite ($Ni_{0.7}Fe_{2.3}O_4$) in SEM-EDS observation. The porosity of crud was controlled from 22% to 31% by increasing heater temperature in the range of 345°C to 355°C. Thermal conductivity of crud decreases by 70% with increasing the porosity to 31%. However, thermal conductivity does not be affected by only crud's porosity. Thermal conductivity of crud was affected by both porosity and surface morphology. It might be because the thermal conductivity of crud is multiply affected by other properties such as surface structure and its thermal stability as well as its porosity. Therefore, it indicates that various structural properties of crud have to be considered together with the porosity to understand well the heat transport of crud at high temperature.

Acknowledgments

This work was financially supported by the National Research Foundation of Korea (NRF) grant funded by the government of the Republic of Korea (2021M2E4A1037979).

REFERENCES

[1] J. Deshon, D. Hyssey, B. Kedrick, J. McGurk, J. Secker, and M. Short, Pressurized Water Reactor Fuel crud and corrosion modeling Nuclear Reactor Power Monitoring, Journal of Materials, 2011

[2] G. Wang, W.A. Byers, M.Y. Young, J. Deshon, Z. Karpitas, and R.L. Oelrich, Thermal conductivity measurements for simulated PWR crud, International Conference on Nuclear Engineering, 2013

[3] J. Deshon, PWR Axial Offset Anomaly (AOA) Guidelines, Rev. 1, EPRI Report, 1008102, EPRI, Palo Alto, 2004.

[4] D. Hussey, D. Wells, Fuel Reliability Guidelines: PWR Fuel Cladding Corrosion and Crud, Rev. 1, EPRI Report, 3002002795, EPRI, Palo Alto, 2014.

[5] J. S. Lee, G. Kim, Crud and Oxide Layer Modeling for Safety Analysis of a PWR, Trans. KNS Spring Meeting, Jeju, Korea, 2016.

[6] J. S Lee, KINS 의 설계기준사고 신안전기준 및 규제검증방법론 개발 현황, Nuclear Safety & Security Information Conf., Deajeon, Korea, 2019.

[7] J. S. Lee, H. D. Jeong, Y. S. Bang, Thermal resistance effects of crud and oxide layers to the safety analysis, Topfuel, 2018.

[8] N. Cinosi, I. Haq, M. Block, S.P. Walker, The effective thermal conductivity of crud and heat transfer from crud-coated PWR fuel, Nuclear Engineering and Design, 792-798, 2011.

[9] S. E. Ziemniak, L. M. Anovitz, R. A. Castelli, W. D. Porter, Magnetic contribution to heat capacity and entropy of nickel ferrite ($NiFe_2O_4$), Journal of Physics and Chemistry of Solids 68, 10-21, 2007.

[10] A.T. Nelson, J. T. White, D.A Andersson, J.A. Aguiar, K.J. McClellan, D.D. Byler, M.P. Short and C.R. Stanek, Thermal expansion, heat capacity, and Thermal conductivity of Nickel ferrite ($NiFe_2O_4$), The American ceramic Society 97, 1559-1565, 2014.